AIAA JOURNAL
Vol. 42, No. 2, February 2004

Evaluation of Radiation Boundary Conditions for the Gust Response Problem

James R. Scott*
NASA John H. Glenn Research Center at Lewis Field, Cleveland, Ohio 44135
and
Kevin L. Kreider† and John A. Heminger‡
University of Akron, Akron, Ohio 44325

The performances of the Sommerfeld, Bayliss–Turkel order-one, and Hagstrom–Hariharan order-one radiation boundary conditions for the single airfoil gust response problem are evaluated. The main objective is to assess quantitatively the accuracy, grid sensitivity, and computational efficiency of each boundary condition. To this end, a matrix of test problems is constructed, and each boundary condition is extensively tested on a large variety of grids. By the use of precise error norms and analytical solutions, it is determined that the Hagstrom–Hariharan condition is the most accurate condition, whereas the Bayliss–Turkel and Hagstrom–Hariharan conditions are about equally insensitive to grid changes. The Sommerfeld and Bayliss–Turkel conditions are the most computationally efficient. Overall, the Bayliss–Turkel condition appears to offer the best combination of accuracy and computational efficiency.

Nomenclature

a_2	=	gust amplitude
c	=	airfoil chord length
c_∞	=	speed of sound
i	=	$\sqrt{-1}$
$\boldsymbol{i}, \boldsymbol{j}$	=	unit vectors in x_1, x_2 directions
k, K	=	Helmholtz frequency
k_1	=	reduced frequency
M	=	Mach number
p	=	unsteady pressure
r, θ	=	polar coordinates
t	=	time
$\boldsymbol{U}$	=	total velocity
U_∞	=	mean velocity
$\boldsymbol{u}_\infty$	=	upstream gust
x, y	=	Prandtl–Glauert coordinates
x_1, x_2	=	streamwise coordinate, transverse coordinate
β	=	$\sqrt{(1 - M^2)}$
η, ξ	=	elliptic coordinates
ρ_∞	=	mean flow density
ϕ	=	unsteady velocity potential
ψ	=	transformed velocity potential

Introduction

THE development of radiation boundary conditions for wave-like equations has been an active and fruitful research area for many years now. This has made available to code developers a large variety of far-field boundary conditions (FFBCs) for use in computational aeroacoustics (CAA) applications. As a result, it has become increasingly important to conduct performance studies to see how well the various conditions work in different applications. It is primarily through this process that the strengths and limitations of the various FFBCs become known. Some recent work on performance evaluation of FFBCs for CAA applications is presented in Refs. 1–9.

In this paper, we are concerned with evaluating radiation boundary conditions for the single airfoil gust response problem. We examine the performance of the Sommerfeld,[10] Bayliss–Turkel[11] order-one, and Hagstrom–Hariharan[12] order-one radiation conditions. Our objective is to assess rigorously the accuracy, grid sensitivity, and computational efficiency of each FFBC.

To this end, we consider the case of a thin airfoil in a transverse gust. We construct a matrix of test problems that includes a large range of Mach numbers and reduced frequencies. For each case in the matrix, we extensively test each boundary condition on a large variety of grids. Using precise error norms and analytical solutions, we determine the accuracy and grid sensitivity of each boundary condition.

Mathematical Formulation

For a flat plate in a periodic vortical gust, the governing equation is

$$\frac{1}{{c_\infty}^2}\frac{\mathrm{D}^2\phi}{\mathrm{D}t^2} - \nabla^2\phi = 0 \tag{1}$$

where

$$\frac{\mathrm{D}}{\mathrm{D}t} = \frac{\partial}{\partial t} + \frac{\partial}{\partial x_1}$$

and ϕ is the unsteady velocity potential. The upstream gust $\boldsymbol{u}_\infty$ is taken to be a single Fourier component of a transverse velocity disturbance and is given by

$$\boldsymbol{u}_\infty = a_2 \exp[ik_1(x_1 - U_\infty t)]\,\boldsymbol{j} \tag{2}$$

The total unsteady velocity $\boldsymbol{U}$ is given by

$$\boldsymbol{U}(\boldsymbol{x}, t) = U_\infty \boldsymbol{i} + \boldsymbol{u}_\infty + \boldsymbol{\nabla}\phi \tag{3}$$

and the unsteady disturbance pressure is obtained from

$$p = -\rho_\infty \frac{\mathrm{D}\phi}{\mathrm{D}t} \tag{4}$$

Presented as Paper 2002-2441 at the AIAA/CEAS 8th Aeroacoustics Conference, Breckenridge, CO, 17 June 2002; received 11 April 2003; revision received 11 September 2003; accepted for publication 24 September 2003.

*Senior Research Scientist, Acoustics Branch, 21000 Brookpark Road; James.R.Scott@nasa.gov. Senior Member AIAA.
†Professor, Department of Theoretical and Applied Mathematics; Kreider@math.uakron.edu.
‡Associate Professor, Department of Theoretical and Applied Mathematics; heminger@amrl.uakron.edu.

At the airfoil surface, ϕ satisfies the impermeability condition

$$\frac{\partial \phi}{\partial x_2} = -a_2 \exp[ik_1(x_1 - U_\infty t)] \tag{5}$$

In the wake ϕ obeys the continuity of pressure condition

$$\frac{\mathrm{D}}{\mathrm{D}t}(\Delta\phi) = 0 \tag{6}$$

where $\Delta\phi$ denotes the jump in ϕ across the wake. Finally, far upstream, ϕ satisfies

$$\nabla\phi \to 0 \tag{7}$$

as $x_1 \to -\infty$.

Numerical Approach

Let the flat plate be coincident with the x_1 axis, centered about the origin. Let lengths be normalized by $c/2$, time by $c/2U_\infty$, ϕ by $(c/2)|a_2|$, a_2 by $|a_2|$, and U_∞ and c_∞ by U_∞. Then the boundary value problem becomes

$$M^2 \frac{\mathrm{D}^2\phi}{\mathrm{D}t^2} - \nabla^2\phi = 0 \tag{8}$$

$$\frac{\partial \phi}{\partial x_2} = -a_2 \exp(ik_1 x_1 - ik_1 t) \tag{9}$$

for $-1 \le x_1 \le 1,\ x_2 = 0$,

$$\frac{\mathrm{D}}{\mathrm{D}t}(\Delta\phi) = 0 \tag{10}$$

for $x_1 > 1,\ x_2 = 0$,

$$\nabla\phi \to 0 \tag{11}$$

as $x_1 \to -\infty$.

When the change of variables is made,

$$x = x_1, \qquad y = \beta x_2 \tag{12a}$$

$$\psi = \phi \exp\left[i\left(k_1 M^2/\beta^2\right)x\right] \exp(ik_1 t) \tag{12b}$$

Equation (8) is transformed into the Helmholtz equation

$$\frac{\partial^2\psi}{\partial x^2} + \frac{\partial^2\psi}{\partial y^2} + K^2\psi = 0 \tag{13a}$$

where

$$K = k_1 M/\beta^2 \tag{13b}$$

Boundary conditions (9–11) become

$$\frac{\partial \psi}{\partial y} = -\frac{a_2}{\beta} \exp\left(ik_1 x/\beta^2\right) \tag{14}$$

for $-1 \le x \le 1,\ y = 0$,

$$\left(-\frac{ik_1}{\beta^2} + \frac{\partial}{\partial x}\right)(\Delta\psi) = 0 \tag{15}$$

for $x > 1,\ y = 0$, and

$$\nabla\psi \to 0 \tag{16}$$

as $x \to -\infty$, respectively.

Because Eqs. (13–16) represent a wave propagation problem, it is important to transform the independent variables into computational coordinates that facilitate the propagation of outgoing waves. The elliptic coordinates (η, ξ), defined by

$$x = \cos(\pi\eta)\cosh(\pi\xi), \qquad y = \sin(\pi\eta)\sinh(\pi\xi) \tag{17}$$

are well suited for this task. The governing equation then becomes

$$\frac{\partial^2\psi}{\partial\eta^2} + \frac{\partial^2\psi}{\partial\xi^2} + \pi^2 K^2[\sin^2(\pi\eta) + \sinh^2(\pi\xi)]\psi = 0 \tag{18}$$

and the boundary conditions are transformed accordingly.

Finally, on selection of an FFBC, the boundary value problem can be discretized in a straightforward manner with finite differences.[13,14] The resulting matrix equation can be solved with a sparse matrix solver.

Radiation Boundary Conditions

We consider the Sommerfeld[10] (Som), Bayliss–Turkel[11] order-one (BT), and Hagstrom–Hariharan[12] order-one (HH) radiation boundary conditions.

The Som radiation condition is

$$\left(\frac{\partial}{\partial r} - ik\right)u = 0 \tag{19}$$

where u satisfies the Helmholtz equation

$$\Delta u + k^2 u = 0 \tag{20}$$

Although the Som condition is exact at infinity, it is known to cause spurious reflections when imposed at a finite distance.[15,16] Equation (19) is accurate to $\mathcal{O}(r^{-3/2})$.

The BT and HH conditions can be expressed conveniently in operator notation. First, let

$$B = i\,k - 1/2r \tag{21}$$

Then the BT condition is

$$\left(\frac{\partial}{\partial r} - B\right)u = 0 \tag{22}$$

Although the BT condition differs from the Som condition only by the $1/2r$ term, its accuracy is, by construction, $\mathcal{O}(r^{-5/2})$, that is, one order higher than the Som condition.

Now let

$$H = ik - 1/r \tag{23a}$$

$$J = -(ik - 1/2r)H + 1/8r^2 \tag{23b}$$

Then the HH condition is

$$\left(J + H\frac{\partial}{\partial r} + \frac{1}{2r^2}\frac{\partial^2}{\partial\theta^2}\right)u = 0 \tag{24}$$

Equation (24) is accurate to $\mathcal{O}(r^{-7/2})$.

Note that the preceding boundary conditions are intended for circular boundaries. The elliptic coordinate transformation (17) provides an outer boundary that is nearly circular for most problems. However, there will be a loss of accuracy as the outer boundary deviates from a circle. Grote and Keller[17] have extended the BT condition to elliptical coordinates, which would be directly applicable to the present work. However, because there is no similar extension[12] for the HH condition, the only head-to-head comparison that can be made is in polar coordinates.

Radiation conditions (19), (22), and (24) can be applied to the transformed potential ψ because ψ satisfies the Helmholtz equation (13). However, it has been observed previously that this does not lead to accurate far-field calculations.[13,14] A far superior approach is to apply the radiation condition to the pressure p, which also satisfies Eq. (13). This leads to an additional operator acting on ψ in the FFBC. From Eq. (4), this operator is

$$\left(\frac{\partial}{\partial x} - A\right) \tag{25a}$$

where

$$A = ik_1/\beta^2 \tag{25b}$$

We may, therefore, identify the variable u in Eqs. (19–24) with the pressure p and write (leaving out the minus sign)

$$u = \left(\frac{\partial}{\partial x} - A\right)\psi \tag{26}$$

The Som, BT, and HH radiation conditions for the unsteady pressure are then

$$\left(\frac{\partial}{\partial r} - iK\right)\left(\frac{\partial}{\partial x} - A\right)\psi = 0 \tag{27}$$

$$\left(\frac{\partial}{\partial r} - B\right)\left(\frac{\partial}{\partial x} - A\right)\psi = 0 \tag{28}$$

$$\left(J + H\frac{\partial}{\partial r} + \frac{1}{2r^2}\frac{\partial^2}{\partial\theta^2}\right)\left(\frac{\partial}{\partial x} - A\right)\psi = 0 \tag{29}$$

respectively, where the frequency k in Eqs. (19–24) is now identified with K as defined in Eq. (13b).

Note that each of the preceding conditions is a local condition, as opposed to the so-called nonlocal conditions such as the Dirichlet-to-Neumann (DtN) map.[15,17] The DtN condition is an exact radiation condition, whereas local conditions such as Eqs. (27–29) are only approximate. However, for a finite difference implementation, local boundary conditions offer the important advantage of preserving the block structure of the matrix. The reader is referred to the recent article by Givoli[18] for a detailed discussion on local and nonlocal radiation boundary conditions.

To implement numerically Eqs. (27–29), all derivatives are recast in (η, ξ) coordinates. For Eqs. (27) and (28), derivatives are evaluated with a rectangular stencil of 12 points, three in the η direction and four in the ξ direction. For Eq. (29), we use a square stencil of 25 points, five in the η direction and five in the ξ direction. A larger stencil is needed for Eq. (29) due to the third-order derivatives. All ξ derivatives are implemented with one-sided backward differencing, and all η derivatives are implemented with central differencing. The implementation is second-order accurate.

Evaluation of Radiation Boundary Conditions

Our main objective is to assess quantitatively the accuracy, grid sensitivity, and computational efficiency of conditions (27–29). To this end, we consider the case of a thin airfoil in a transverse gust. This problem has an exact solution, so that the accuracy of numerical calculations can be precisely determined.

In the construction of a comprehensive test of the boundary conditions, the following effects should be included: 1) variations in Mach number and reduced frequency, 2) variations in the Helmholtz constant K defined in Eq. (13b), and 3) variations in grid size and spacing. To satisfy effects 1 and 2, we consider a matrix of test problems where the Mach number M ranges from 0.1 to 0.5 to 0.8, and the reduced frequency k_1 assumes values of 0.1, 0.5, 1.0, 2.0, and 3.0. This provides 15 different Mach number/reduced frequency combinations, with K ranging from 0.0101 to 6.67.

To satisfy effect 3, we solve each problem in the test matrix on 15 different grids. The grids vary in their tangential spacing and in the location of their outer grid boundary. The spacing in the radial direction is kept fixed at 24 points per wavelength. Each grid is designed to provide an accurate calculation, so that differences in accuracy will be due to the FFBC. Details on the construction of accurate grids for the gust response problem are found in Refs. 14 and 19.

All calculations are performed using the GUST3D code,[14,19,20] a second-order accurate finite difference code. Two parameters in the code are used to specify the grids. The parameter neta specifies the number of η grid points, and the parameter nwaves specifies the distance to the outer grid boundary in terms of gust wavelengths. Tables 1 and 2 list the different grid configurations.

Table 1 Grid parameters for $k_1 = 0.1$, 0.5, and 1.0

Grid number	neta	nwaves
1	31	3.0
2	31	3.5
3	31	4.0
4	31	4.5
5	31	5.0
6	36	3.0
7	36	3.5
8	36	4.0
9	36	4.5
10	36	5.0
11	41	3.0
12	41	3.5
13	41	4.0
14	41	4.5
15	41	5.0

Table 2 Grid parameters for $k_1 = 2.0$ and 3.0

Grid number	neta	nwaves
1	41	5.0
2	41	5.5
3	41	6.0
4	41	6.5
5	41	7.0
6	46	5.0
7	46	5.5
8	46	6.0
9	46	6.5
10	46	7.0
11	51	5.0
12	51	5.5
13	51	6.0
14	51	6.5
15	51	7.0

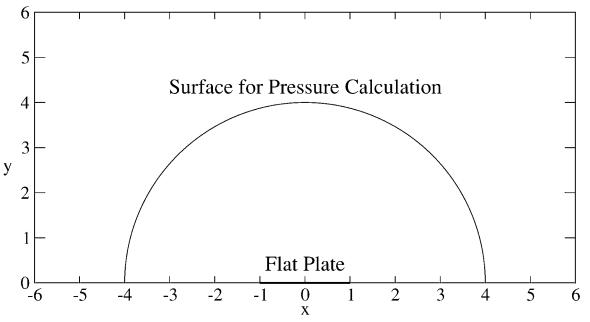

Fig. 1 Semicircle of radius two chord lengths for far-field pressure calculation.

Note that neta is the number of η grid points in the upper half-plane because GUST3D solves the problem only in that region due to symmetry. Also, neta and nwaves are bigger for $k_1 = 2.0$ and 3.0 due to the shorter gust wavelength for these cases.

As a metric for assessment of the accuracy of numerical results, we compare computed and exact pressure values on a semicircle of radius two chord lengths, centered about the airfoil center, as shown in Fig. 1. In Figs. 2 and 3, we show comparisons between computed and exact pressures on this semicircle for two typical cases.

The error of numerical calculations is quantified with the absolute ℓ_∞ and relative ℓ_2 norms. The absolute ℓ_∞ error is calculated by

$$\max_n \left| P^n_{\text{comp}} - P^n_{\text{ex}} \right|, \qquad n = 0, 1, \ldots, 360$$

where the semicircle is discretized by 361 uniformly spaced points and P^n_{comp} and P^n_{ex} are the computed and exact pressure at point n,

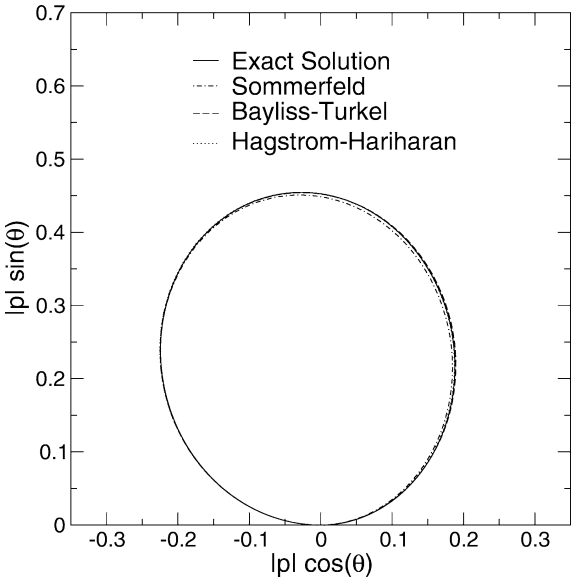

Fig. 2 Comparison of far-field pressure on semicircle of radius two chord lengths: $M = 0.5$, $k_1 = 1.0$, flat plate in a transverse gust.

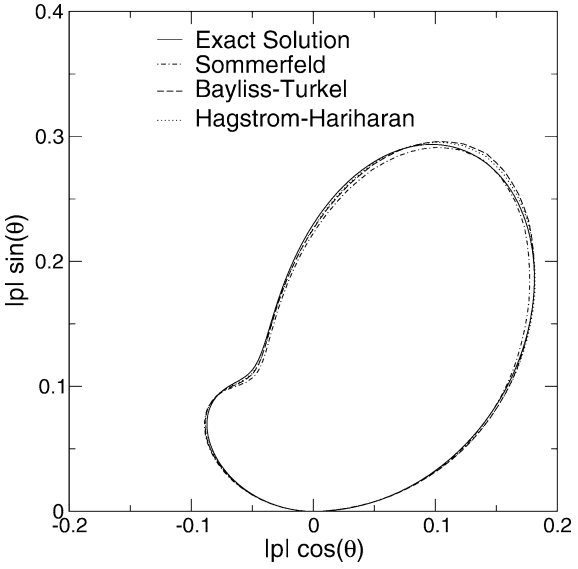

Fig. 3 Comparison of far-field pressure on semicircle of radius two chord lengths: $M = 0.5$, $k_1 = 3.0$, flat plate in a transverse gust.

respectively. The relative ℓ_2 error is calculated by

$$\frac{\sqrt{\Sigma_{n=0}^{360}\left(P_{\text{comp}}^{n} - P_{\text{ex}}^{n}\right)^2}}{\sqrt{\Sigma_{n=0}^{360}\left(P_{\text{ex}}^{n}\right)^2}}$$

The absolute ℓ_∞ norm measures the worst pointwise local error, whereas the relative ℓ_2 norm measures the overall accuracy across the whole semicircle. Both measures are needed to assess fully the accuracy of numerical results. For example, a large ℓ_∞ error indicates at least one point where the computed pressure is inaccurate, but it provides no information about accuracy at the other points.

In Figs. 4–8, we show the relative ℓ_2 error for all three boundary conditions for the 0.5 Mach number case. These are presented as typical results, whereas results for the other cases in the test matrix are omitted for brevity. Note from Figs. 4–8 that the Som condition is significantly less accurate and more sensitive to grid changes than either the BT or HH conditions. Also note that the error tends to be periodic with the far-field boundary location for all three boundary conditions.

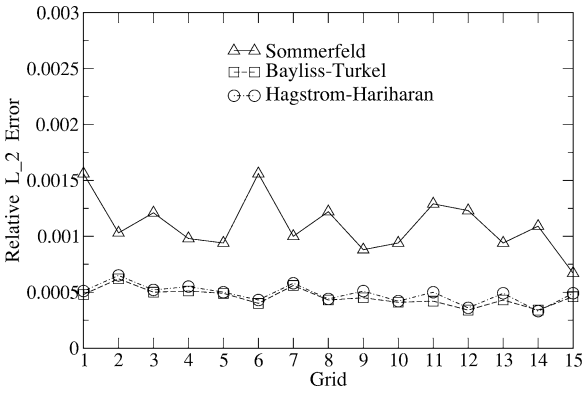

Fig. 4 Relative ℓ_2 error for $M = 0.5$ and $k_1 = 0.1$.

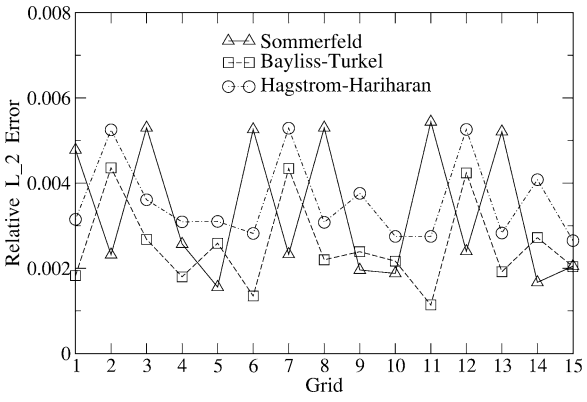

Fig. 5 Relative ℓ_2 error for $M = 0.5$ and $k_1 = 0.5$.

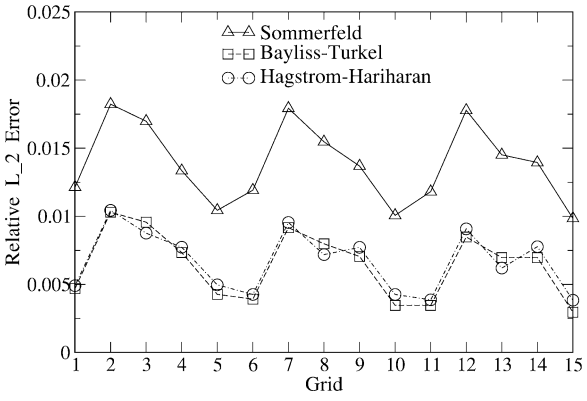

Fig. 6 Relative ℓ_2 error for $M = 0.5$ and $k_1 = 1.0$.

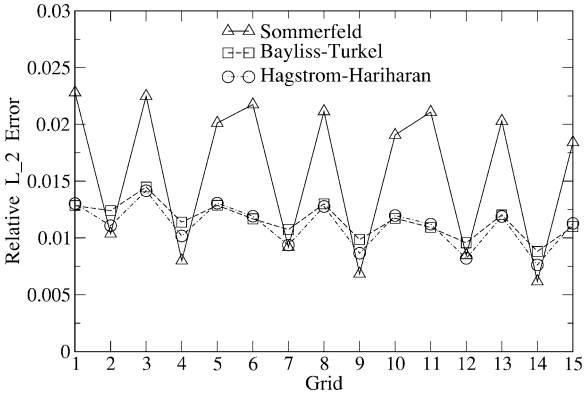

Fig. 7 Relative ℓ_2 error for $M = 0.5$ and $k_1 = 2.0$.

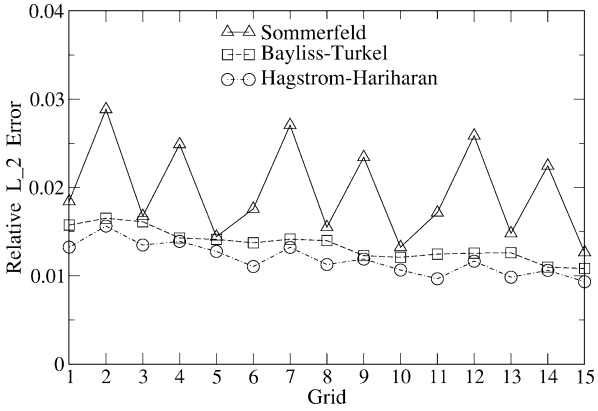

Fig. 8 Relative ℓ_2 error for $M = 0.5$ and $k_1 = 3.0$.

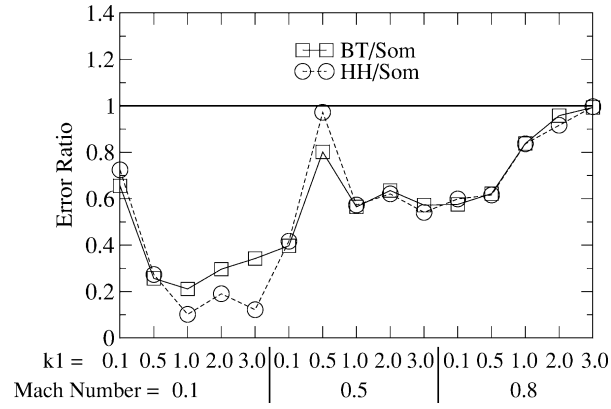

Fig. 9 Ratio of max relative ℓ_2 error for all cases in the test matrix.

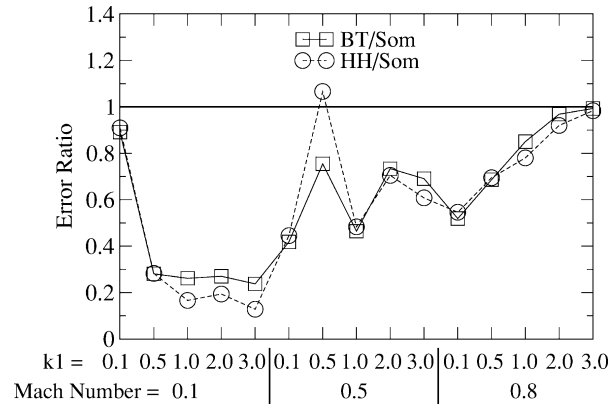

Fig. 10 Ratio of mean relative ℓ_2 error for all cases in the test matrix.

To quantify the overall performance of each boundary condition, we calculate the following three quantities for each case in the test matrix: 1) the maximum error of the 15 calculations for each case, 2) the mean error of the 15 calculations, and 3) the standard deviation of the error. We do this for both the relative ℓ_2 and absolute ℓ_∞ error. Figures 9–11 show how the boundary conditions compare by the use of the ℓ_2 error, and Figs. 12–14 show how they compare by the use of the ℓ_∞ error. To facilitate the comparison, the BT and HH results are shown as a ratio to the Som results.

From Figs. 9–14, one can make the following conclusions: 1) Both the BT and HH conditions are far superior to the Som condition for the $M = 0.1$ case, with the HH condition being best overall. 2) For $M = 0.5$, the BT and HH conditions are significantly better than Som for all reduced frequencies, except $k_1 = 0.5$. 3) For $M = 0.8$, the BT and HH conditions are significantly better than Som only for $k_1 = 0.1$, 0.5, and 1.0. 4) For high-Mach-number, high

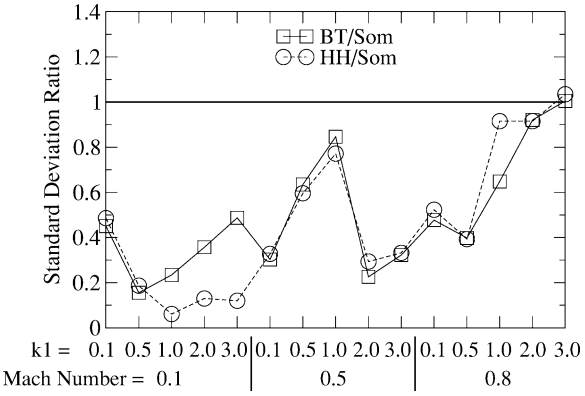

Fig. 11 Ratio of relative ℓ_2 standard deviation for all cases in the test matrix.

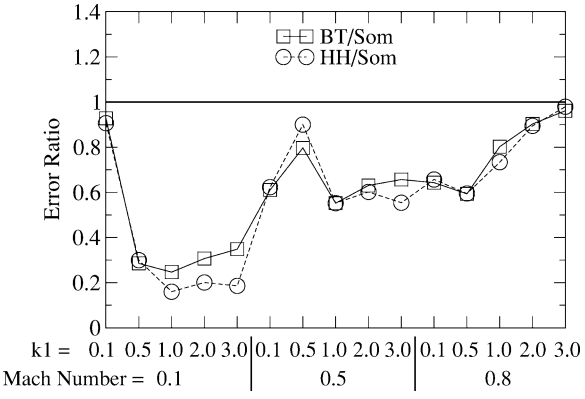

Fig. 12 Ratio of maximum absolute ℓ_∞ error for all cases in the test matrix.

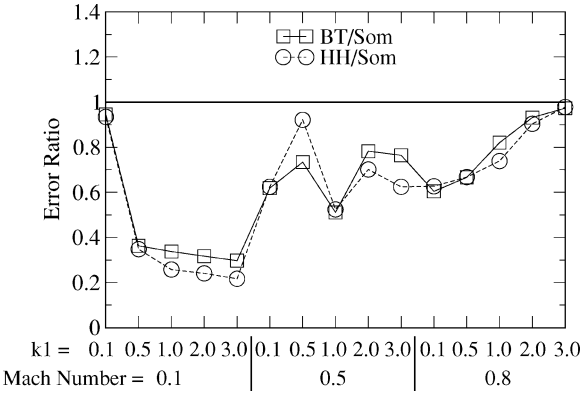

Fig. 13 Ratio of mean absolute ℓ_∞ error for all cases in the test matrix.

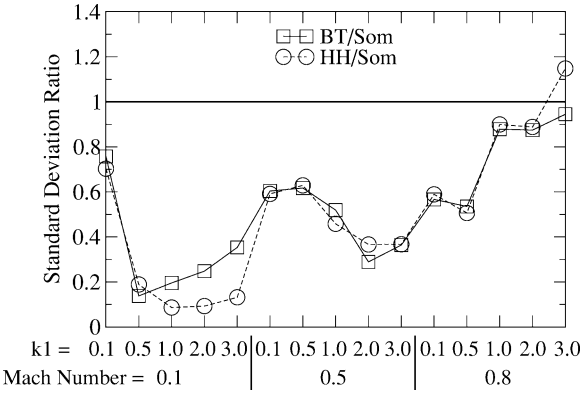

Fig. 14 Ratio of absolute ℓ_∞ standard deviation for all cases in the test matrix.

Table 3 Best far-field boundary condition based on relative ℓ_2 error

M	k_1	Maximum error	Mean error	Standard deviation
0.1	0.1	BT	BT	BT
0.1	0.5	BT	BT	BT
0.1	1.0	HH	HH	HH
0.1	2.0	HH	HH	HH
0.1	3.0	HH	HH	HH
0.5	0.1	BT	BT	BT
0.5	0.5	BT	BT	HH
0.5	1.0	BT	BT	HH
0.5	2.0	HH	HH	BT
0.5	3.0	HH	HH	BT
0.8	0.1	BT	BT	BT
0.8	0.5	HH	BT	HH
0.8	1.0	HH	HH	BT
0.8	2.0	HH	HH	HH
0.8	3.0	BT	HH	Som

Table 4 Best far-field boundary condition based on absolulte ℓ_∞ error

M	k_1	Maximum error	Mean error	Standard deviation
0.1	0.1	HH	HH	HH
0.1	0.5	BT	HH	BT
0.1	1.0	HH	HH	HH
0.1	2.0	HH	HH	HH
0.1	3.0	HH	HH	HH
0.5	0.1	BT	BT	HH
0.5	0.5	BT	BT	BT
0.5	1.0	BT	BT	HH
0.5	2.0	HH	HH	BT
0.5	3.0	HH	HH	BT
0.8	0.1	BT	BT	BT
0.8	0.5	BT	BT	HH
0.8	1.0	HH	HH	BT
0.8	2.0	HH	HH	BT
0.8	3.0	BT	BT	BT

reduced-frequency cases, the Som condition performs as well as the BT and HH conditions.

Along with the preceding conclusions, it is also useful to summarize which boundary condition performs the best for the different cases in the test matrix. In Tables 3 and 4, we summarize which FFBC is best in terms of the smallest maximum error, smallest mean error, and smallest standard deviation. Table 3 presents results based on relative ℓ_2 error, whereas Table 4 presents results based on absolute ℓ_∞ error.

From Tables 3 and 4, one finds that in the categories of smallest maximum error and smallest mean error, the HH condition is best 33 out of 60 times, whereas the BT condition is best 27 times. In the category of smallest standard deviation, the BT condition is best 15 out of 30 times, whereas the HH condition is best 14 times. We conclude that the HH condition is the most accurate and that the BT and HH conditions are about equally insensitive to grid changes.

In terms of computational efficiency, the Som and BT conditions are nearly identical. The HH condition is the least efficient, requiring about 7% more CPU time and about 33% more storage than the other conditions. This is because of the larger discretization stencil required at the outer grid boundary, which leads to a fuller matrix during the Gaussian elimination process. However, note that the larger stencil is required only because of the third derivative terms that appear in Eq. (29) due to the pressure operator defined in Eq. (25a). Without the pressure operator, the three boundary conditions could be implemented with the same stencil and still maintain second-order accuracy. This leads us to expect that, in problems where the additional operator is not needed, the HH condition would be superior in accuracy and also comparable in efficiency to the other methods.

Summary

In this paper, a detailed study of the Som, BT order-one, and HH order-one radiation boundary conditions is carried out. Each boundary condition is evaluated on a matrix of test problems with three different Mach numbers and five different reduced frequencies. It is determined that the HH condition is most accurate and that the BT and HH conditions are least sensitive to grid changes. The Som condition performs as well as the BT and HH conditions for high Mach number, high reduced-frequency cases. Finally, for the problem at hand, the BT condition appears to offer the best combination of accuracy and computational efficiency.

Acknowledgment

The second and third authors gratefully acknowledge support for this work provided by NASA Grant NCC3-765.

References

[1]Scott, J. N., Mankbadi, R. R., Hayder, M. E., and Hariharan, S. I., "Outflow Boundary Conditions for the Computational Analysis of Jet Noise," AIAA Paper 93-4366, Oct. 1993.

[2]Hixon, R., Shih, S.-H., and Mankbadi, R. R., "Evaluation of Boundary Conditions for Computational Aeroacoustics," *AIAA Journal*, Vol. 33, No. 11, 1995, pp. 2006–2012.

[3]Hayder, M., and Turkel, E., "Nonreflecting Boundary Conditions for Jet Flow Computations," *AIAA Journal*, Vol. 33, No. 12, 1995, pp. 2264–2270.

[4]Goodrich, J. W., and Hagstrom, T., "A Comparison of Two Accurate Boundary Treatments for Computational Aeroacoustics," AIAA Paper 97-1585, May 1997.

[5]Hagstrom, T., and Goodrich, J. W., "Experiments with Approximate Radiation Boundary Conditions for Computational Aeroacoustics," *Applied Numerical Mathematics*, Vol. 27, 1998, pp. 385–402.

[6]Qi, Q., and Geers, T. L., "Evaluation of the Perfectly Matched Layer for Computational Acoustics," *Journal of Computational Physics,* Vol. 139, 1998, pp. 166–183.

[7]Cloudhari, M., Li, F., and Tam, C. K. W., "Numerical Boundary Conditions for Simulation of Gust–Cascade Interaction," AIAA Paper 99-1845, May 1999.

[8]Dietiker, J.-F., Hoffman, K. A., and Forsythe, J. R., "Assessment of Computational Boundary Conditions for Hyperbolic Systems," AIAA Paper 99-3350, Jan. 1999.

[9]Hixon, R., Shih, S.-H., and Mankbadi, R. R., "Evaluation of Boundary Conditions for the Gust–Cascade Problem," *Journal of Propulsion and Power*, Vol. 16, No. 1, 2000, pp. 72–78.

[10]Sommerfeld, A., *Partial Differential Equations in Physics*, Academic Press, New York, 1964, p. 189.

[11]Bayliss, A., and Turkel, E., "Radiation Boundary Conditions for Wave-Like Equations," *Communications in Pure and Applied Mathematics*, Vol. 33, 1980, pp. 707–725.

[12]Hagstrom, T., and Hariharan, S. I., "A Formulation of Asymptotic and Exact Boundary Conditions Using Local Operators," *Applied Numerical Mathematics*, Vol. 27, 1998, pp. 403–416.

[13]Scott, J. R., and Atassi, H. M., "Numerical Solution of Periodic Vortical Flows About a Thin Airfoil," NASA TM 101998, June 1989.

[14]Scott, J. R., and Atassi, H. M., "A Finite-Difference, Frequency-Domain Numerical Scheme for the Solution of the Gust Response Problem," *Journal of Computational Physics*, Vol. 119, 1995, pp. 75–93.

[15]Keller, J. B., and Givoli, D., "Exact Non-Reflecting Boundary Conditions," *Journal of Computational Physics*, Vol. 82, 1989, pp. 172–192.

[16]Bayliss, A., Gunzburger, M., and Turkel, E., "Boundary Conditions for the Numerical Solution of Elliptic Equations in Exterior Regions," *SIAM Journal on Applied Mathematics*, Vol. 42, No. 2, 1982, pp. 430–451.

[17]Grote, M. J., and Keller, J. B., "On Nonreflecting Boundary Conditions," *Journal of Computational Physics*, Vol. 122, 1995, pp. 231–243.

[18]Givoli, D., "High-Order Nonreflecting Boundary Conditions Without High-Order Derivatives," *Journal of Computational Physics*, Vol. 170, 2001, pp. 849–870.

[19]Scott, J. R., and Atassi, H. M., "High Frequency Gust Interaction with Single Loaded Airfoils in Subsonic Flows" *Proceedings of the Sixth International Symposium on Unsteady Aerodynamics, Aeroacoustics and Aeroelasticity of Turbomachines and Propellers*, edited by H. M. Atassi, Springer-Verlag, New York, 1991, pp. 743–764.

[20]Scott, J. R., and Atassi, H. M., "Numerical Solutions of the Linearized Euler Equations for Unsteady Vortical Flows Around Lifting Airfoils," AIAA Paper 90-0694, Jan. 1990.

W. Devenport
Associate Editor